Inorg. Chem. **2006**, *45*, 7133–7143

Insight into the Catalytic Mechanism of Vanadium Haloperoxidases. DFT Investigation of Vanadium Cofactor Reactivity

Giuseppe Zampella,[†] Piercarlo Fantucci,[†] Vincent L. Pecoraro,*[,‡] and Luca De Gioia*[,†]

Department of Biotechnology and Biosciences, University of Milano-Bicocca, Piazza della Scienza 2, 20126 Milano, Italy, and Department of Chemistry, University of Michigan, Ann Arbor, Michigan 48109-1055

Received April 3, 2006

Density functional theory (DFT) has been used to investigate the catalytic properties of the *isolated* vanadium cofactor found in vanadium haloperoxidases, with a particular emphasis on the steps going from the resting form of the cofactor to the peroxo complex. Computation of transition states, intermediate species, and UV–vis spectra, as well as comparison of reaction energies, demonstrated the important role of protonation in cofactor activation. This illustrates that the resting form of the vanadium cofactor reacts with hydrogen peroxide according to a mechanism that implies formation of an aqua complex, release of the apical water molecule according to a dissociative pathway, and binding of hydrogen peroxide to vanadium. This process leads to a side-on peroxo species corresponding to the peroxo form observed in the enzyme. In addition, it appears that an acid–base catalysts strongly accelerates the conversion to the side-on peroxo form. The comparison of computed and experimental UV–vis spectra corroborated the proposed reaction pathway and allowed us to explain the effects of the vanadium ligands on the electronic properties of the cofactor.

Introduction

The catalytic properties of vanadium haloperoxidases (VHPOs), which are enzymes that catalyze the oxidation of halide ions by hydrogen peroxide to the corresponding hypohalous acids, have been extensively investigated in recent years.[1] X-ray diffraction data collected on the resting and peroxo forms of VHPOs (Figure 1),[2−5] as well as kinetic and spectroscopic investigations of the enzymatic system, have disclosed many relevant aspects related to the catalytic mechanism and to structure−function relationships.[6−9] The chemistry of vanadium complexes related to the enzyme active site is well developed.[10−25] In fact, several peroxo-

* To whom correspondence should be addressed. E-mail: vlpec@umich.edu (V.L.P.); luca.degioia@unimib.it (L.D.G.).
[†] University of Milano-Bicocca.
[‡] University of Michigan.

(1) de Boer, E.; Wever, R. *J. Biol. Chem.* **1988**, *263*, 12326−12332. Van Schijndel, J. W. P. M.; Barnet, P.; Roelse, J.; Vollenbroek, E. G. M.; Wever, R. *Eur. J. Biochem.* **1994**, *225*, 151−157. Everett, R. R.; Soedjak, H. S.; Butler, A. *J. Biol. Chem.* **1990**, *265*, 15671−15679. Butler, A. *Coord. Chem. Rev.* **1999**, *187*, 17−35. Arber, J. M.; de Boer, E.; Garner, C. D.; Hasnain, S. S.; Wever, R. *Biochemistry* **1989**, *28*, 7968−7973. Butler, A. *Science* **1998**, *281*, 207.
(2) Messerschmidt, A.; Wever, R. *Proc. Natl. Acad. Sci. U.S.A.* **1996**, *93*, 392−396.
(3) Messerschmidt, A.; Prade, L.; Wever, R. *Biol. Chem.* **1997**, *378*, 309−315.
(4) Weyand, M.; Hecht, H.-J.; Kie, M.; Liaud, M.-F.; Vilter, H.; Schomburg, D. *J. Mol. Biol.* **1999**, *293*, 596−611.
(5) Isupov, M. N.; Dalby, A. R.; Brindley, A. A.; Izumi, Y.; Tanabe, T.; Murshudov, G. N.; Littlechild, J. A. *J. Mol. Biol.* **2000**, *299*, 1035−1049.
(6) Hemrika, W.; Renirie, R.; Macedo-Ribeiro, S.; Messerschmidt, A.; Wever, R. *J. Biol. Chem.* **1999**, *274*, 23820−23827.
(7) Macedo-Ribeiro, S.; Hemrika, W.; Renirie, R.; Wever, R.; Messerschmidt, A. *J. Biol. Inorg. Chem.* **1999**, *4*, 209−219.
(8) Casny, M.; Rehder, D.; Schmidt, H.; Vilter, H.; Conte, V. *J. Inorg. Biochem.* **2000**, *80*, 157−160.
(9) Renirie, R.; Hemrika, W.; Pierma, S. R.; Wever, R. *Biochemistry* **2000**, *39*, 1133−1141.
(10) Clague, M. J.; Keder, N. L.; Butler, A. *Inorg. Chem.* **1993**, *32*, 4754−4761.
(11) Martinez, J. S.; Carrol, G. L.; Tschirret-Guth, R. A.; Altenhoff, G.; Little, R. D.; Butler, A. *J. Am. Chem. Soc.* **2001**, *123*, 3289−3294.
(12) Slebodnick, C.; Hamstra, B. J.; Pecoraro, V. L. In *Metal Sites in Proteins and Models*; Sandler, P. J., Ed.; Springer-Verlag: Berlin, 1997; Vol. 89, pp 51−108.
(13) (a) Rehder, D. *Inorg. Chem. Commun.* **2003**, *6*, 604−617. (b) Rehder, D. *Coord. Chem. Rev.* **1999**, *182*, 297−322.
(14) Mimoun, H.; Saussine, L.; Daire, E.; Postel, M.; Fischer, J.; Weiss, R. *J. Am. Chem. Soc.* **1983**, *105*, 3101.
(15) Butler, A.; Clague, M. J.; Meister, G. E. *Chem. Rev.* **1994**, *94*, 625−638.
(16) (a) Bortolini, O.; Di Furia, F.; Scrimin, P.; Modena, G. *J. Mol. Catal.* **1980**, *7*, 147. (b) Bortolini, O.; Conte, V.; Di Furia, F.; Modena, G. *Nouv. J. Chim.* **1985**, *9*, 147.
(17) Ballistreri, F. P.; Tomasselli, G. A.; Toscano, R. M.; Conte, V.; Di Furia, F. *J. Am. Chem. Soc.* **1991**, *113*, 6209.
(18) Smith, T. S., II; Pecoraro, V. L. *Inorg. Chem.* **2002**, *41*, 6754−6760.
(19) Plass, W. *Coord. Chem. Rev.* **2003**, *237*, 205−212.

10.1021/ic060555g CCC: $33.50
Published on Web 08/02/2006

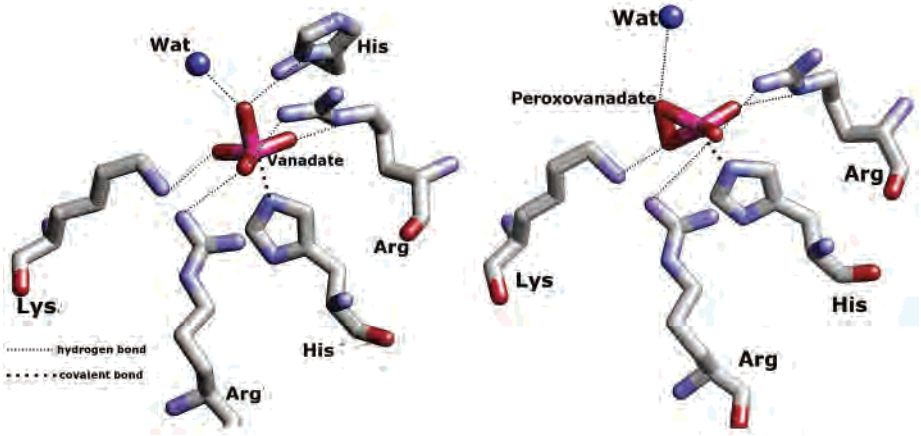

Figure 1. X-ray structures of the native (left) and peroxo (right) forms of the VCPO cofactor. The surrounding amino acid residues, along with the near most crystallization water molecule, are also shown.

vanadium complexes are capable of carrying out a variety of oxidation/oxygen transfer reactions: sulfides are converted to sulfoxides and sulfones,[17,18,26−29] hydrocarbons can be hydroxylated[14] and halogenated,[10,11,30] olefins are turned into epoxides,[16a] and alcohols are oxidized to aldehydes and ketones.[16b]

Experimental investigations have been recently complemented by computational studies,[31−38] which led to a better understanding of the catalytic properties of the enzyme. In particular, experimental and computational results converge on a scenario in which the vanadium cofactor in the resting state of the enzyme can be described as an equilibrium between a trigonal bipyramidal vanadate species featuring hydroxyl groups in equatorial and axial position and another configuration with an axial water and three equatorial oxo moieties. In addition, protonation of the resting cofactor leads to a configuration containing an axial water and one hydroxo group in the equatorial plane.[37] As for the active peroxo species, it has been shown that protonation plays a key role in formation and activation of peroxo-vanadium model complexes.[39,40] Moreover, oxo-transfer to the substrate should involve the unprotonated axial peroxo oxygen atom.[32,36]

Despite significant recent progresses, key issues related to the catalytic mechanism of the enzyme are still not fully understood. In fact, UV−vis spectroscopy data[9] indicate that the resting form of vanadium cofactor is quite rapidly transformed to the peroxo state upon H_2O_2 addition. However, little is known about the reaction coordinate connecting the resting form of the cofactor to the active peroxo form. Kinetic investigations on functional synthetic models suggest an associative mechanism for the process leading to peroxo species formation.[40] Aqua-ligated species may also be formed when using excess amount of acid during turnover.[40a] As for the protein, Messerschmidt et al. have proposed a dissociative mechanism in which aqua-ligated species are likely to play a role.[3,6]

In addition, the role of H^+ in the conversion from the resting to the peroxo form of the enzyme and related synthetic complexes is not fully understood. The investigation of biomimetic models shows that protonation of the resting form is crucial for efficient conversion to the peroxo form.[40a] However, kinetic investigations carried out on the enzyme show that conversion from resting to peroxo form is slower at pH 5.0 than at pH 8.3.[9]

Quantum chemical methods are important tools for inspecting both transition metal chemistry[41] and properties of catalytic sites of metallo-enzymes.[42] Herein, we have used density functional theory (DFT) to investigate crucial issues

(20) Ligtenbarg, A. G. J.; Hage, R.; Feringa, B. L. *Coord. Chem. Rev.* **2003**, *237*, 89−101.
(21) Ligtenbarg, A. G. J. Vanadium and Iron Complexes for Catalytic Oxidation, Ph.D. Thesis, 2001.
(22) Crans, D. C.; Keramidas, A. D.; Hoover-Litty, H.; Anderson, O. P.; Miller, M. M.; Lemoine, L. M.; Pleasic-Williams, S.; Vandenberg, M.; Rossomando, A. J.; Sweet, L. *J. Am. Chem. Soc.* **1997**, *119*, 9 (23), 5447−5448.
(23) Crans, D. C.; Smee, J. J.; Gaidamauskas, E.; Yang, L. *Chem. Rev.* **2004**, *104* (2), 849−902.
(24) Santoni, G.; Licini, G.; Rehder, D. *Chem. Eur. J.* **2003**, *9*, 4700−4708.
(25) Bortolini, O.; Conte, V. *J. Inorg. Biochem.* **2005**, *99*, 1549−1557.
(26) ten Brink, H. B.; Tuynman, A.; Dekker: H. L.; Hemrika, W.; Izumi, Y.; Oshiro, T.; Schoemaker, H. E.; Wever, R. *Inorg. Chem.* **1998**, *37*, 6780−6784.
(27) ten Brink, H. B.; Holland, H. L.; Schoemaker, H. E.; von Lingen, H.; Wever, R. *Tetrahedron: Asymmetry* **1999**, *10*, 4563−4572.
(28) Andersson, M. A.; Willets, A.; Allenmark, S. G. *J. Org. Chem.* **1997**, *62*, 8455−8458.
(29) Andersson, M. A.; Allenmark, S. G. *Tetrahedron* **1998**, *54*, 15293−15304.
(30) Carter-Franklin, J. N.; Parrish, J. D.; Tschirret-Guth, R. A.; Little, R. D.; Butler, A. *J. Am. Chem. Soc.* **2003**, *125*, 3688−3689.
(31) Zampella, G.; Yudenfreund Kravitz, J.; Webster, C. E.; Fantucci, P.; Hall, M. B.; Carlson, H. A.; Pecoraro, V. L.; De Gioia, L. *Inorg. Chem.* **2004**, *43*, 4127−4136.
(32) Zampella, G.; Fantucci, P.; Pecoraro, V. L.; De Gioia, L. *J. Am. Chem. Soc.* **2005**, *127*, 953−960.
(33) Buhl, M. *J. Comput. Chem.* **1999**, *20*, 1254−1261.
(34) Buhl, M.; Schurhammer, R.; Imhof, P. *J. Am. Chem. Soc.* **2004**, *126* (10), 3310−3320.
(35) Conte, V.; Bartolini, O.; Carraro, M.; Moro, S. *J. Inorg. Biochem.* **2000**, *80*, 41−49.
(36) Balcells, D.; Maseras, F.; Lledos, A. *J. Org. Chem.* **2003**, *68*, 4265−4274.
(37) Kravitz, J. Y.; Pecoraro, V. L.; Carlson, H. A. *J. Chem. Theory Comput.* **2005**, *1*, 1265−1274.
(38) Raugei, S.; Carloni, P. *J. Phys. Chem. B* **2005**, *110*, 3747.
(39) Colpas, G. J.; Hamstra, B. J.; Kampf, J. W.; Pecoraro, V. L. *J. Am. Chem. Soc.* **1996**, *118*, 3469−3478.
(40) (a) Hamstra, B. J.; Colpas, G. J.; Pecoraro, V. L. *Inorg. Chem.* **1998**, *37*, 949−955. (b) Wieghardt, K. *Inorg. Chem.* **1978**, *17*, 57. (c) Funahashi, S.; Haraguchi, K.; Tanaka, M. *Inorg. Chem.* **1977**, *16*, 1349.
(41) Niu, S.; Hall, M. B. *Chem. Rev.* **2000**, *100*, 353−405. Ziegler, T.; Autschbach, J. *Chem. Rev.* **2005**, *105*, 2695.

related to the catalytic mechanism of vanadium haloperoxidases, with a specific emphasis on the steps going from the native form of the cofactor to the active peroxo complex. In particular, one of the main goals of the present investigation was the elucidation of key properties of the *isolated* cofactor of VHPOs. In fact, the thorough characterization of the vanadium cofactor structure−function relationships in the whole protein is very difficult, using both experimental and theoretical approaches. On the other hand, to the best of our knowledge, synthetic models resembling exactly the vanadium coordination sphere observed in the enzyme are still elusive. Therefore, a clear picture of the intrinsic reactivity of the vanadium cofactor with H_2O_2, which is a necessary prerequisite to fully understand the catalytic activity of the enzyme, is still lacking. Moreover, the elucidation of the catalytic properties of the *isolated* vanadium cofactor might drive the synthesis of novel synthetic catalysts.

UV−vis spectra of some species proposed to be formed in the catalytic pathway have also been computed and compared to experimental data, also to highlight possible analogies between solution [8,9] and crystallographic[2] species.

Methods

DFT structure optimizations were performed using both pure B-P86[43] and hybrid B3-LYP[44] functionals, associated to an all-electron valence triple-ζ basis set with polarization functions on all atoms (TZVP).[45] Calculations have been carried out using the Turbomole suite of programs.[46] The resolution of the identity technique[47,48] was exploited for approximating the four-center bielectronic integrals in the B-P86 method.

Optimization of the transition state structures has been carried out according to a pseudo-Newton−Raphson method. Initially, geometry optimization of a guessed transition state structure is performed with constrained degrees of freedom constituting the reaction coordinate. The initial Hessian have been calculated at the classical level, whereas the B-P86/RI/TZVP and B3-LYP/TZVP were used to compute the final Hessian matrix of the minimum energy structure. Vibrational analysis of the minimum energy structures was carried out and, after finding a stationary point characterized by an imaginary frequency associated with the reaction coordinate, the curvature determined at such point was used to begin the transition state search. Transition state structures were sought by using an eigenvector-following procedure.

Calculation of analytical second derivatives of DFT energy allowed us to characterize each stationary point. Potential energy barriers were computed by considering as reactants the energy optimized adducts of the starting materials. Approximated rotational and vibrational partition functions were computed for every stationary point in order to get Gibbs free energy values directly from the electronic energy.

Scheme 1. Stoichiometry for the Reaction between the Resting Vanadium Cofactor and Hydrogen Peroxide

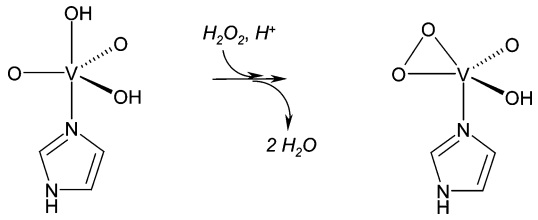

Energy barriers for proton-transfer steps involving a water molecule were computed as the difference between the energy of the transition state and the energy of the van der Waals adduct between the reactant and a water molecule.

Ground-state molecular orbitals were used to obtain the energies of the low-lying singlet → singlet transitions, computed as vertical excitations, using the ESCF package within the time-dependent DFT formalism.[49] Both B-P86 and B3-LYP functionals have been used to compute UV−vis spectra, but since results are similar, only B3-LYP spectra are shown in the following discussion. Computed UV spectra have been obtained centering the Gaussian curves with amplitude = 10 nm on the transition frequencies. Computed electronic transitions are available as Supporting Information.

Environmental effects were modeled by using the COSMO[50] method, as implemented in Turbomole. The dielectric constant, ϵ, was set to 40, a suitable value to simulate the effect of charge−charge interactions typical of protein active sites featuring polar amino acids.[50,51]

Results

In light of the X-ray structures of the resting[2,4] and peroxo[3] forms of vanadium haloperoxidases (see Figure 1), the reaction between hydrogen peroxide and the resting form of the enzyme cofactor $[V(OH)_2(O)_2Im]^-$ implies a stoichiometry consistent with protonation and replacement of two water molecules (Scheme 1).

To fully characterize the reactivity properties of the *isolated* resting cofactor ($[V(OH)_2(O)_2Im]^-$), different pathways for its reaction with hydrogen peroxide have been investigated. It turned out that the reaction between $[V(OH)_2(O)_2Im]^-$ and H_2O_2 cannot easily take place, neither according to a dissociative nor an associative mechanism. On one hand, intermediate species and transition states for direct attack of hydrogen peroxide to the metal cofactor could not be found, ruling out an associative pathway. On the other hand, dissociative paths corresponding to V−OH bond cleavage are, as expected, extremely endoergonic. We have also sampled the possibility that $[V(OH)_2(O)_2Im]^-$ could react with OOH^-. It turned out that the hydroperoxide anion is more basic than $[V(OH)_2(O)_2Im]^-$, leading to H_2O_2 and

(42) Siegbahn, P. E. M.; Blomberg, M. R. A.*Chem. Rev.* **2000**, *100*, 421−437. Lovell, T.; Himo, F.; Han, W.-G.; Noodleman, L. *Coord. Chem. Rev.* **2003**, *238*−*239*, 211. Friesner, R. A.; Baik, M.-H.; Gherman, B. F.; Guallar, V.; Wirtam, M.; Murphy, R. B.; Lippard, S. J. *Coord. Chem. Rev.* **2003**, *238*−*239*, 267.
(43) Becke, A. D. *Phys. Rev. A* **1988**, *38*, 3098. Perdew, J. P. *Phys. Rev. B* **1986**, *33*, 8822.
(44) Lee, C.; Yang, W.; Parr, R. G.; *Phys Rev. B* **1988**, *37*, 785−789.
(45) Schafer, A.; Huber, C.; Ahlrichs, R. *J. Chem. Phys.* **1994**, *100*, 5829.
(46) Ahlrichs, R.; Bar, M.; Haser, M.; Horn, C.; Kolmel, C. *Chem. Phys. Lett.* **1989**, *162*, 165.
(47) Eichkorn, K.; Treutler, O.; Öhm, H.; Haser, M.; Ahlrichs, R. *Chem. Phys. Lett.* **1995**, *240*, 283.
(48) Eichkorn, K.; Weigend, F.; Treutler, O.; Ahlrichs, R. *Theor. Chem. Acc.* **1997**, *97*, 119.
(49) Furche, F. *J. Chem. Phys.* **2001**, *114*, 5982. Furche, F.; Ahlrichs, R. *J. Chem. Phys*. **2002** *117*, 7433. Dreuw, A.; Head-Gordon, M. *Chem. Rev.* **2005**, *105* (11), 4009−4037.
(50) (a) Klamnt, A. *J. Phys. Chem*. **1995**, *99*, 2224. (b) Klamnt, A. *J. Phys. Chem*. **1996**, *100*, 3349.
(51) (a) Warshel, A.; Naray-Szabo, G.; Sussman, F.; Hwang, j.-K. *Biochemistry* **1989**, *28*, 3629. (b) Bottoni, A.; Lanza, C. Z.; Miscione, G. P.; Spinelli, D. *J. Am. Chem. Soc*. **2004**, *126*, 1542−1550.

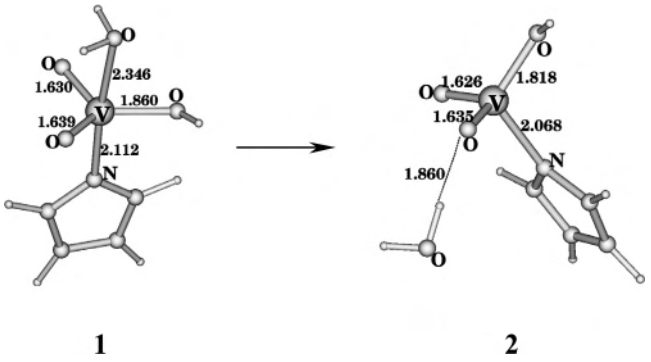

Figure 2. Energy-optimized structures of reactants and products for water loss from the protonated form of the native cofactor. Distances are given in Å.

Scheme 2. Reaction between **1** and H_2O_2 According to Associative and Dissociative Pathways

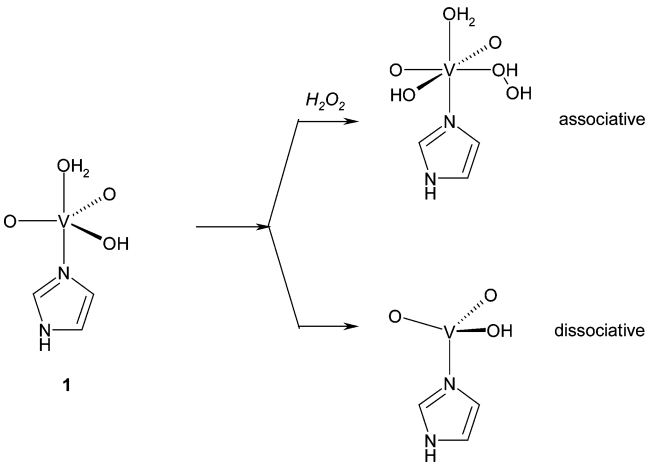

$[V(OH)(O)_3Im]^{2-}$, which spontaneously decomposes due to cleavage of the V−Im bond.

It should be noted that kinetic studies on synthetic functional models have often pointed out the role of protonation in labilizing oxo/hydroxo ligands of vanadium complexes, thus allowing hydrogen peroxide binding.[40] Indeed, protonation accelerates the reaction between H_2O_2 and biomimetic vanadium complexes.[1,23,39] In this context, QM/MM studies have shown that protonation of the resting form of the cofactor leads to a species containing an axial water and one hydroxo group in the equatorial plane.[37] Furthermore, DFT optimization of $[V(H_2O)(OH)(O)_2Im]$ (**1**; Figure 2), using both B-P86 and B3-LYP functionals, resulted in stable structures with extremely similar geometries, as deduced by differences between corresponding bond lengths and angles, which are lower than 0.025 Å and 3°, respectively (data not shown). Very similar structures were obtained with B-P86 and B3LYP for all intermediates and transition states discussed in the present work. As a consequence, all geometry parameters will be hereafter referred to the B-P86 results.

The reaction between **1** and H_2O_2 can, at least in principle, take place either according to an associative or a dissociative reaction pathway (Scheme 2).

All attempts to obtain six-coordinated vanadium species in which H_2O_2 and H_2O were simultaneously coordinated to vanadium resulted in cleavage of V−O bonds and formation of five-coordinated complexes. Moreover, any attempt to locate a transition state structure for concerted peroxide attack and water release from vanadium failed. Analogous results were obtained for the reaction between **1** and OOH^- taking place according to an associative mechanism (not shown). On the other hand, a dissociative mechanism may be operative. Release of the apical water molecule from **1** is slightly exoergonic (Table 1) and results in the formation of the tetrahedral intermediate species $[V(OH)(O)_2Im]$ (**2**; Figure 2). Interaction of H_2O_2 with the tetrahedral vanadium complex (**3**; Figure 3) goes through the transition state structure **TS3-4** and eventually evolves to **4**.

Table 1. Reaction Energies and Barriers (kcal mol^{-1}) for Reaction Steps Relevant to the Catalytic Mechanism of VHPOs[a]

ΔG, $\Delta G^{\ddagger}$	B-P86 $\epsilon = 1$	B-P86 $\epsilon = 40$	B3-LYP $\epsilon = 1$	B3-LYP $\epsilon = 40$
1 → 2	−3.2	−5.6	−1.9	−3.7
3 → TS3-4	5.2	6.6	6.8	3.0
3 → 4	2.1	4.9	6.7	2.9
4 → TS4-5	14.7	14.5	19.2	18.5
4 → TS4-5w	0	1.2	5.0	7.4
4 → 5	−5.4	−1.4	−4.2	0
5 → 6	1.5	0.9	0.5	−1.4
6 → TS6-7	5.7	5.1	10.9	12.4
6 → TS6-7w	1.1	0.1	5.6	7.7
6 → 7	−10.6	−12.5	−10.0	−10.6
8 → TS8-2	16.9	14.4	20.1	17.1
8 → TS8-2w	7.5	6.2	11.3	9.6
8 → 2	1.2	−1.5	−0.2	−3.8
8 → TS8-9	22.7	24.3	26.5	25.5
8 → TS8-9w	24.9	23.7	31.4	29.9
8 → 9	3.5	6.2	2.7	6.0
9 → TS9-1	17.6	15.0	21.5	18.3
9 → TS9-1w	4.6	0.1	8.1	4.1
9 → 1	5.0	−0.9	5.0	−2.2

[a] "w" labels indicate $\Delta G^{\ddagger}$ values computed in the presence of a water molecule mediating proton transfer.

In **4**, the vanadium ion has a trigonal bipyramidal geometry and H_2O_2 is bound apically in an end-on fashion. The conversion **3 → 4** is only slightly endoergonic, and the energy barrier associated to the transition state **TS3-4** is low (Table 1).

The H_2O_2−V species **4** spontaneously converts to **5** (Table 1), in which a proton has moved from the peroxo OH group coordinated to vanadium to one of the equatorial oxo groups. Deprotonation of the coordinated H_2O_2 moiety results in a very large contraction of the axial V−O bond (from 2.369 to 1.846 Å; Figure 4).

It is worth noting that proton transfer from H_2O_2 to the equatorial oxo group in **4** could take place directly, going through the transition state structure **TS4-5** (Figure 4). However, the energy barrier is larger than 14 kcal mol^{-1} due to the transient formation of a strained four-member ring. On the other hand, if proton transfer is mediated by a water molecule (**TS4-5w**; Figure 4) the barrier becomes very low, decreasing by more than 10 kcal mol^{-1} (Table 1). Remarkably, the analysis of the X-ray structure of vanadium haloperoxidase from *Ascophyllum nodosum* reveals that a water molecule (W772) is close to the metal cofactor and has the proper spatial disposition to act as an acid−base catalyst (Figure 1).[4]

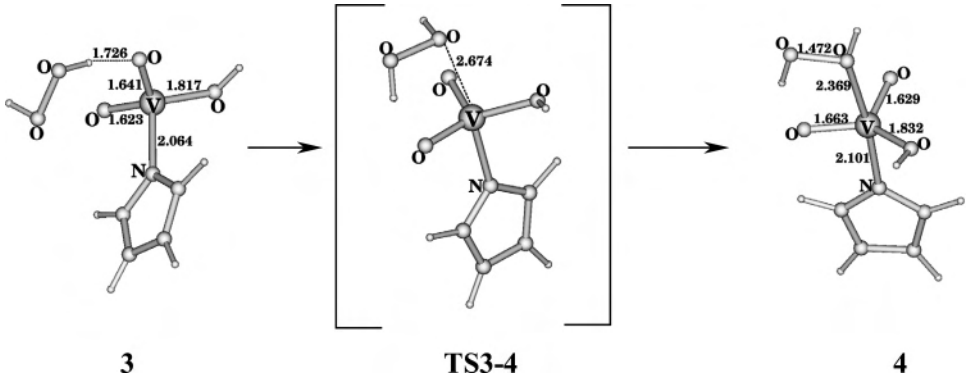

Figure 3. Energy-optimized structures of reactants, transition states, and products for the H_2O_2 binding step to vanadate. Only distances related to the reaction coordinate have been shown in the transition state.

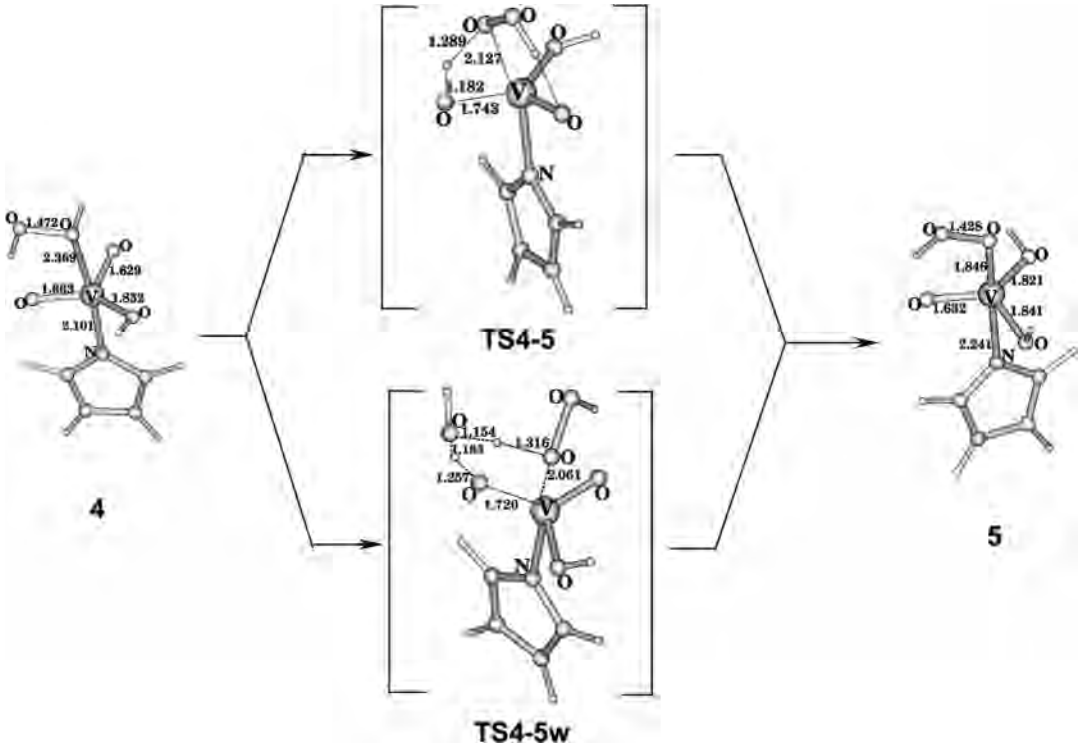

Figure 4. Energy-optimized structures of reactants, transition states, and products for intramolecular proton transfer from H_2O_2 to an equatorial oxygen of the cofactor. The structure of **TS4-5** is rotated along the N−V bond axis by 120° relative to **4**, **TS4-5w**, and **5** to show all structural features of the reaction coordinate.

The end-on isomer **5** is almost isoenergetic to the side-on form **6** (Table 1) in which both peroxo oxygen atoms are coordinated to vanadium (Figure 5).

Release of a water molecule from the vanadium coordination environment in **6** leads to **7**, which is characterized by structural features closely resembling the peroxo form of the cofactor in the enzyme (Figure 6).[3,32]

Notably, the conversion **6** → **7**, which implies proton transfer from the hydroperoxo moiety to an equatorial hydroxo group, is strongly exoergonic (Table 1). Also in this case the energy barrier for the intramolecular proton transfer is high (**TS6**−**7**; Figure 6 and Table 1) due to the transient formation of a four-member ring. However, the involvement of a water molecule in the proton-transfer step, acting as a general acid−base catalyst, decreases significantly the barrier (**TS6**−**7w**; Figure 6 and Table 1).

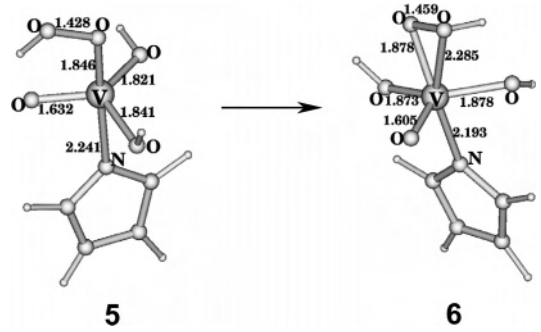

Figure 5. Energy-optimized structures of the end-on (**5**) and side-on (**6**) hydroperoxide species.

In a previous study, it was shown that protonation of the peroxo form of the vanadate cofactor is a prerequisite for its activation and that the oxo-transfer step involves the unprotonated peroxo oxygen atom.[32] It was also shown that

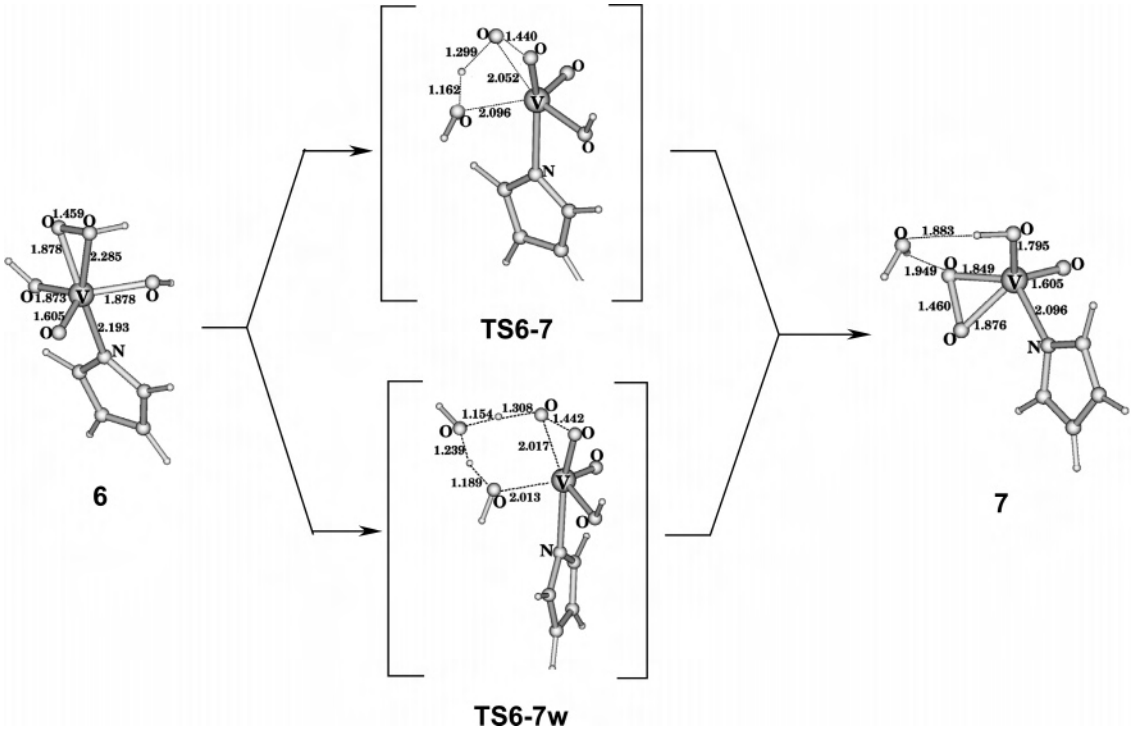

Figure 6. Energy-optimized structures of reactants, transition states, and products for the water release step from the side-on hydroperoxide complex **6** to yield the peroxo form of the cofactor **7**.

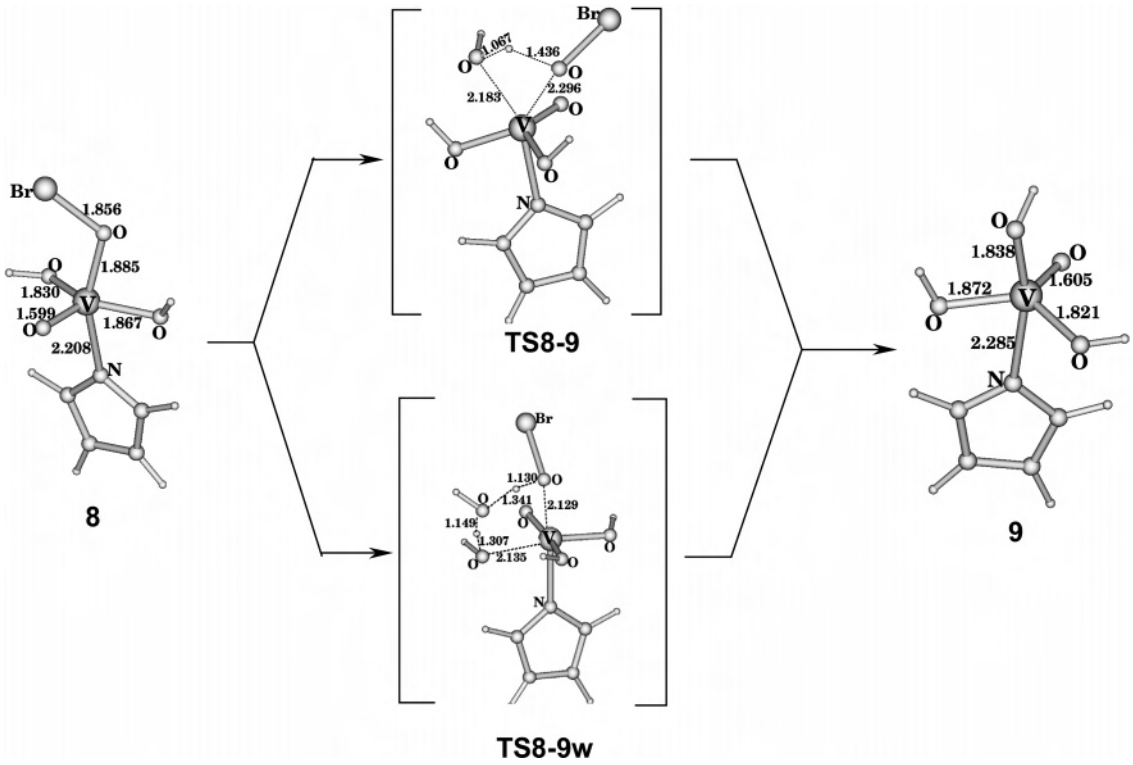

Figure 7. Energy-optimized structures of reactants, transition states, and products for the HOBr release step, according to an associative pathway. Hypohalous acid formation (and release) is accompanied by water coordination to V. HOBr is not shown in the products for the sake of clarity.

when Br^- is the substrate, the reaction with the peroxo form of the cofactor eventually leads to transient formation of the hypobromite adduct **8**, in which the BrO^- group is axially coordinated (Figures 7 and 9). To close the catalytic cycle, hypobromite must be replaced by a water molecule, a reaction step that can in principle take place according to different reaction channels (Scheme 3).

In **TS8-9** (Figure 7), which corresponds to an associative pathway, water binds to vanadium. Proton transfer to BrO^- and release of HBrO takes place simultaneously.

The barrier associated to the transition state **TS8-9** is extremely large (Figure 7; Table 1). A similarly large barrier is found in the reaction pathway going through the transition state **TS8-9w** (Figure 7) in which H_2O binding and HBrO

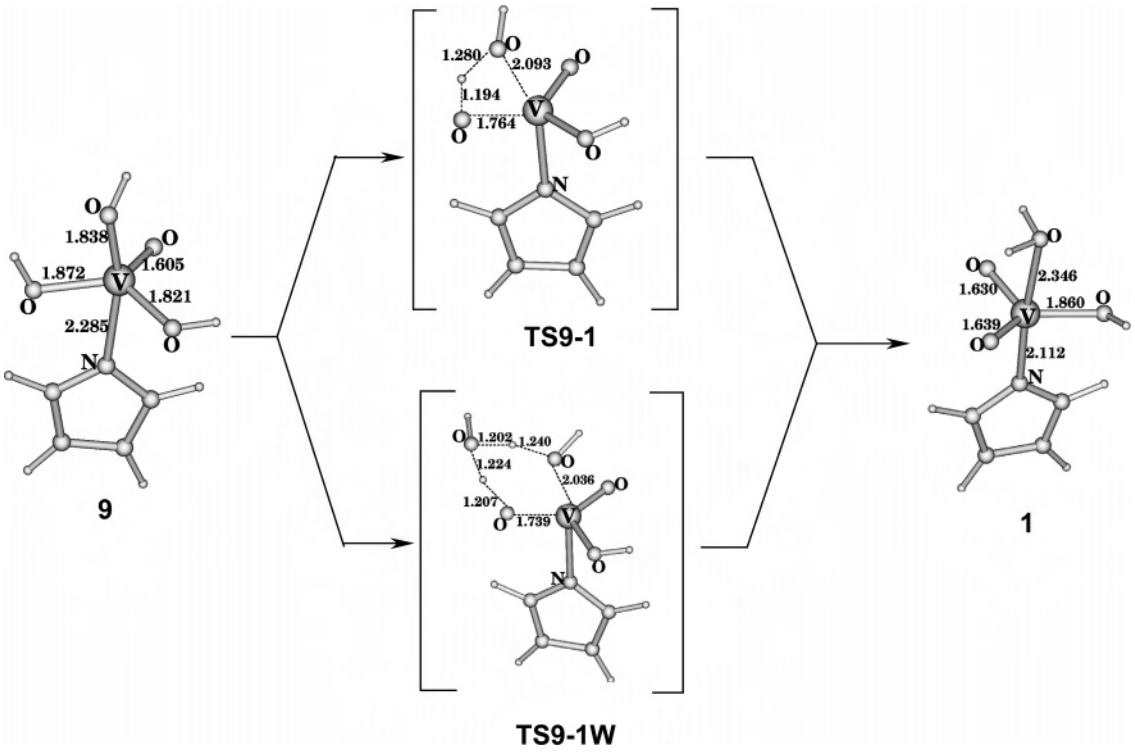

Figure 8. Energy-optimized structures of reactants, transition states, and products for the intramolecular proton transfer leading to the protonated form of the cofactor (**1**).

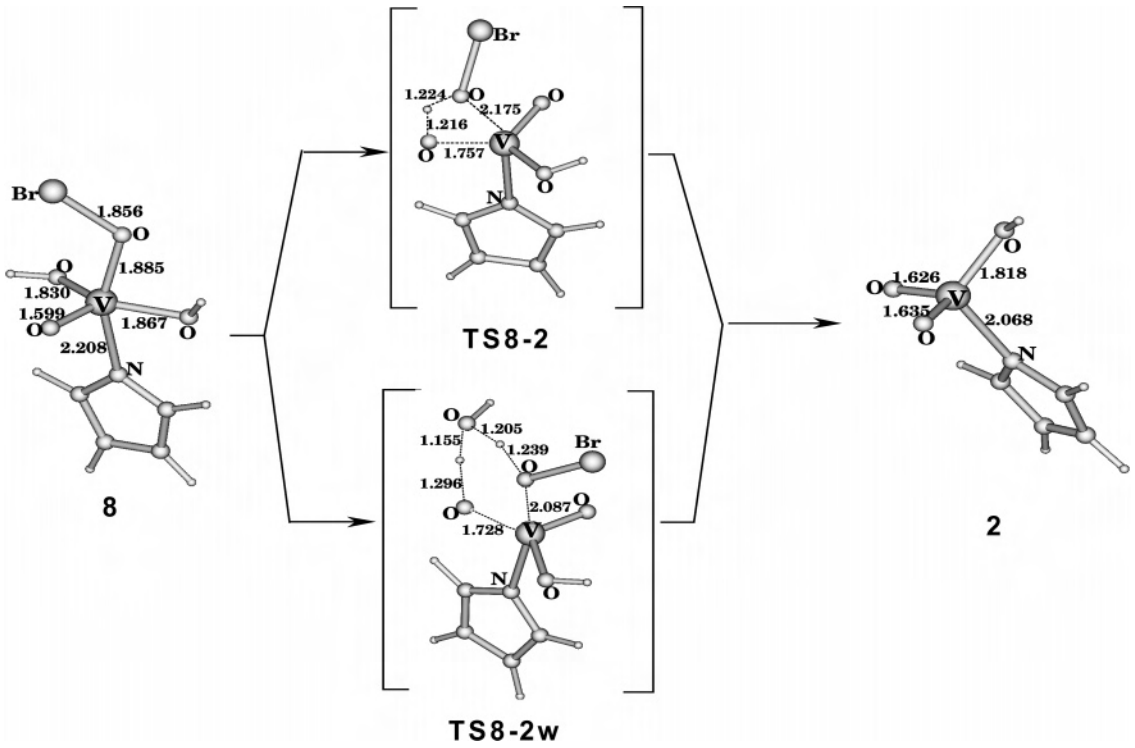

Figure 9. Energy-optimized structures of reactants, transition states, and products for the intramolecular proton transfer from an equatorial oxygen to the axial hypobromite, leading to HOBr release (not shown in the products for the sake of clarity).

release are still simultaneous but proton transfer from H_2O to BrO^- is mediated by an external water molecule. Therefore, an associative mechanism for the substitution of BrO^- by water (**8** → **9**) turns out to be kinetically hindered and thermodynamically slightly disfavored (see Table 1). Tautomerization of **9** could lead to **1**, thus closing the cycle (Figure 8). This step is endoergonic in a vacuum, whereas it becomes slightly exoergonic when considering solvation effects. Moreover, as noted in the other proton-transfer steps, the involvement of a water molecule (**TS9-1w**) decreases significantly the energy barrier relative to the intramolecular proton transfer (**TS9-1**; see Table 1).

A dissociative mechanism for BrO^- release from **8** that implies proton transfer from an equatorial hydroxo group to

Scheme 3. Reaction between **8** and H_2O, According to Associative and Dissociative Pathways

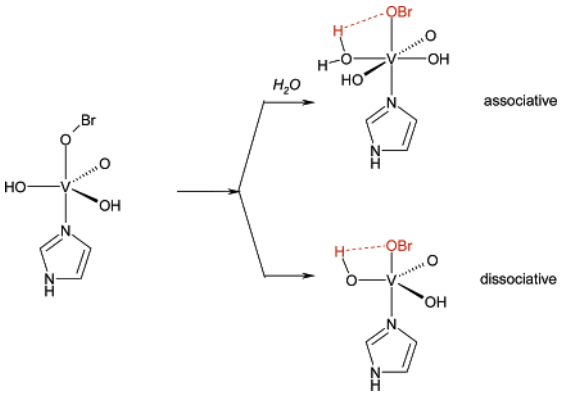

BrO^- (**TS8-2**; Figure 9) is also characterized by a large barrier. However, when H^+ transfer is mediated by a water molecule (**TS8-2w**; Figure 9), the barrier becomes significantly lower than for the other HBrO release pathways (Table 1).

UV−Vis Spectra. Stopped-flow UV−vis spectroscopy has been shown to be a suitable tool for the characterization of intermediate species formed in the conversion of the resting state of VHPOs to the peroxo form.[9] Therefore, to corroborate our mechanicistic proposals, we have computed the UV−vis electronic transitions of the optimized intermediate species involved in the catalytic cycle (Figure 10), comparing theoretical results with available experimental data. Computational data may also help in clarifying the molecular features of the species that have been characterized spectroscopically.[9]

The UV−vis spectrum computed for $[V(OH)_2(O)_2Im]^-$, which corresponds to the resting form of the cofactor characterized by X-ray diffraction (hereafter referred to as **X-ray$_r$**), closely resembles the experimental one, which is characterized by a maximum absorption at 315 nm. It is noteworthy that the blue-shift of the maximum absorption of about 20−30 nm observed when carrying out the UV−vis analysis at acidic pH[9] is nicely reproduced in the computed spectra of **1**, which is formed by protonation of **X-ray$_r$** (Figure 10). Notably, the tetrahedral vanadate species **2**, which forms spontaneously from **1** (Table 1) features a UV−vis spectrum that is not characterized by a maximum absorption around 300 nm.

DFT results are also consistent with a scenario in which peroxo species formation (**7**) is accompanied by disappearance of the intense band at 315 nm, typical of the native form of the cofactor, in very good agreement with experimental data.[9] Notably, computed UV−vis spectra of transiently formed intermediate species (**4**, **5**, **6**) reveal rich spectroscopic features in the 300−380 nm spectral range.

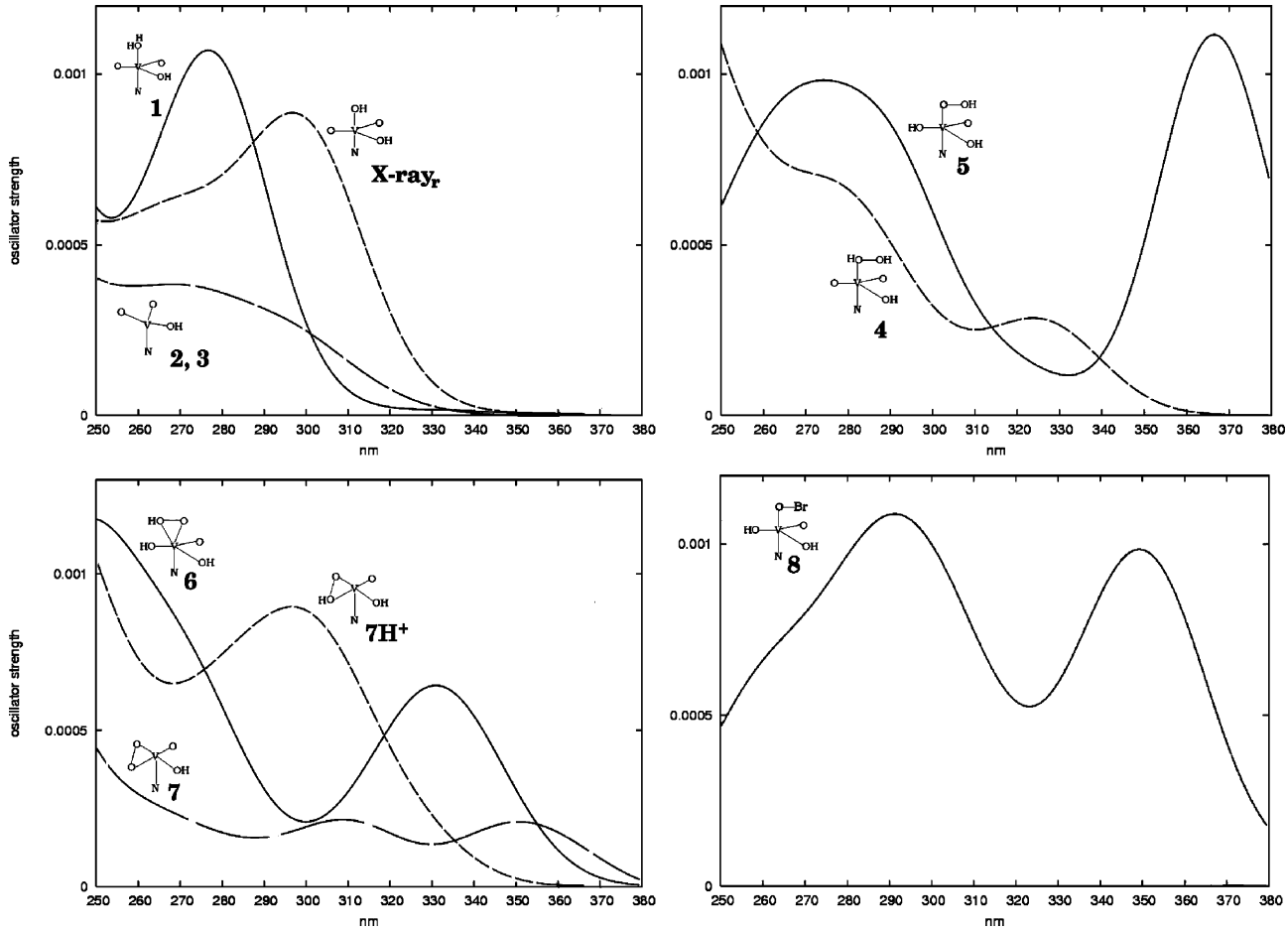

Figure 10. Computed UV−vis spectra of intermediate species formed in the catalytic cycle of VHPOs.

Scheme 4. Mechanism of Halide Oxidation Catalyzed by VHPOs

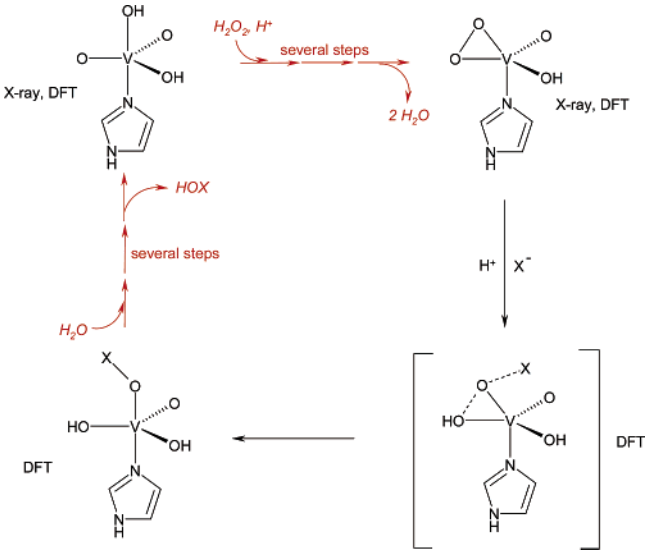

The same holds true for the initial product of Br^- oxidation (**8**), which is characterized by a UV−vis absorption at 350 nm.

Discussion

The elucidation of the catalytic mechanism of VHPOs and related synthetic complexes is extremely important to unravel structure−function relationships in the enzyme and to drive the design of novel and efficient synthetic catalysts. However, while the oxo-transfer step from the peroxo form of the cofactor to the substrate has been thoroughly studied,[32,34,36] much less is known about other molecular details of the catalytic cycle, such as the conversion from the native to the peroxo form, as well as the steps following substrate oxidation and leading to closure of the catalytic cycle (Scheme 4). Moreover, key steps are still controversial. As an example, Raugei and Carloni[38] have recently suggested that the mechanism proposed by Messerschmidt and Wever,[3,6] which implies formation of aquavanadate species, could not be operative in the enzyme.

With the aim of highlighting the reactivity characteristics of the *isolated* vanadium cofactor, we have initially investigated different paths for the reaction between hydrogen peroxide and the resting form of the cofactor. The resting state has been extensively characterized by spectroscopic and computational methods and corresponds to a five-coordinate vanadium (+5) complex, featuring histidine and hydroxide ligation in axial position and two oxo and one hydroxo groups in the equatorial plane.

The investigation of a relatively small system such as the *isolated* vanadium cofactor allowed us to sample thoroughly all plausible reaction paths with hydrogen peroxide (Scheme 5). Notably, it turned out that the only feasible pathway implies initial protonation of the resting form of the vanadium cofactor, with formation of the aqua complex **1**, release of the apical water molecule according to a dissociative pathway (**2**), and eventual binding of hydrogen peroxide to vanadium (**3**; see also Figures 2 and 3). Indeed, protonation of the resting cofactor was proposed to be crucial for the formation of the peroxo active form in functional synthetic models.[1,23,39] Therefore, our results provide a further molecular explanation for the suggestion by Hamstra et al.[40a] concerning the role of acid−base catalysis, not only to protonation/activation of peroxo complex toward halide oxidation but also to favor the hydrogen peroxide binding to vanadium.

Notably, both associative and dissociative mechanisms have been postulated for the protonation of the vanadium peroxo species.[3,6,40] However, we were unable to characterize transition states or intermediate species featuring six ligands in the coordination sphere of vanadium. This result might be qualitatively explained considering the small size of vanadium in its formal +5 redox state, which allows the coordination of only a limited number of ligands. This observation does not contradict the experimental observations indicating that most synthetic model complexes of VHPO can react with hydrogen peroxide according to an associative mechanism. In fact, synthetic complexes are invariably characterized by polydentate ligands,[13,20,21,23] which should

Scheme 5. Reactivity Paths for the Reaction between $[V(OH)_2(O)_2Im]^-$ and H_2O_2 Investigated by DFT Calculations

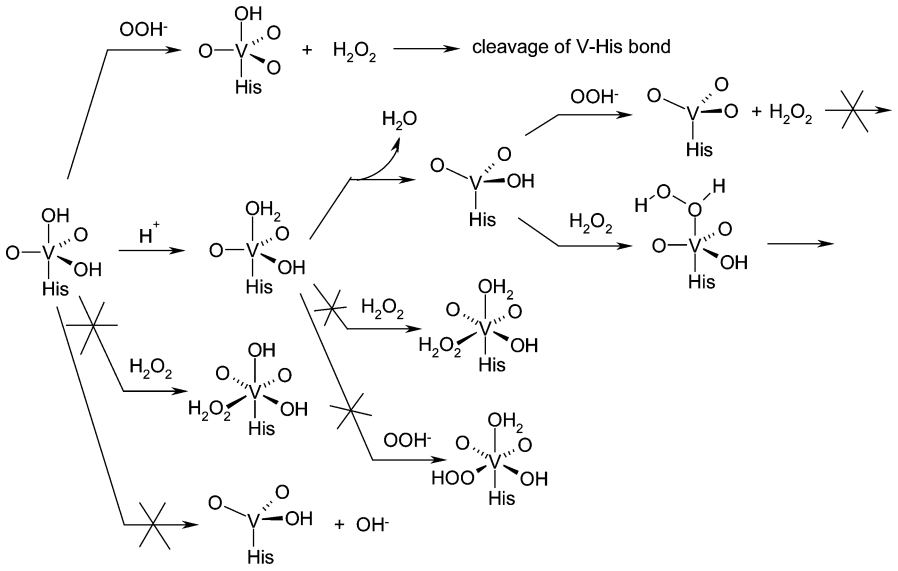

favor associative reaction pathways. It must be also pointed out that we did not find any transition state structure corresponding to H_2O_2 binding to vanadium and simultaneous H_2O (or OH^-) leaving, as recently reported on the basis of hybrid Car−Parrinello/MD calculations carried out on the enzyme.[38] In fact, Raugei and Carloni characterized a low-energy path featuring a transition state structure characterized by a $V-O_{axial}$ interatomic distance of about 3.8 Å. Indeed, such a very long $V-O_{axial}$ distance indicates that hydrogen peroxide is not involved in bonding interaction with the vanadium atom,[52] a scenario that is in full agreement with our data supporting a dissociative mechanism.

Once formed, the $V-H_2O_2$ adduct evolves spontaneously to the side-on peroxo complex **7** going through the transient intermediate species **5** in which hydroperoxo is coordinated in an end-on fashion and **6** in which the hydroperoxo moiety is coordinated in a side-on fashion.

Our results highlight the importance of an acid−base shuttle (here modeled as a water molecule) in lowering the activation barrier for intramolecular proton transfers (see Table 1). Indeed, proton shuttles other than water may be similarly effective in catalyzing proton transfer. Very good candidates for this role in the protein are His418 and H_2-O772 (numbering scheme is from the X-ray structure of *A. nodosum* enzyme). These observations can also be relevant for the design of functional synthetic models of the enzyme, providing useful suggestions about acid−base moieties that might be inserted directly into the molecular framework of the catalyst or, as an alternative, acid−base co-catalysts (or even solvent) to be adopted for such a goal.

Notably, the side-on peroxo species **7**, which corresponds to the X-ray solved structure,[3] is the most stable species among those occurring after hydrogen peroxide coordination to vanadium. The relative instability of both end-on and side-on hydroperoxide vanadium species, relative to the peroxo one, which was proposed on the basis of spectroscopic[8] and theoretical data,[38] is fully confirmed by our calculations.

The effects of H_2O_2 addition to the VHPO cofactor were probed experimentally by stopped-flow UV−vis absorption spectroscopy,[9] observing a clear difference between the spectra of holo- and apo-enzymes. The holo form is characterized by a band at 315 nm, which was shown not to be due to absorption of free vanadate, whereas the peroxo form is not characterized by absorption over 300 nm. Other details are worth noting: no bands in the 300−400 nm region were observed in the H496A mutant, highlighting a possible marked effect of axial histidine on the UV−vis spectral features. Moreover, the R360A protein shows a UV−vis band with the absorption maximum shifted to 305 nm, suggesting that charged amino acids in the cofactor environment could affect significantly its electronic properties. The analysis of computed UV−vis spectra (Figure 10) reveals that there is a good correspondence between the experimental data collected for the resting form of the mutated R360A enzyme and the spectrum computed for **X-ray$_r$**, confirming the marked influence of the apical histidine and the subtle effect of equatorial amino acids (see Figure 1) on the electronic spectra of the cofactor. Moreover, the close correspondence between the computed spectral features of **X-ray$_r$** (which corresponds to the structure of the cofactor observed in the crystal) and the UV−vis spectra collected in solution for the resting form, strongly suggests that the structure of the cofactor is the same in solution and the solid state.

In the resting form of the protein, the UV−vis band at 315 nm is shifted toward 305 nm moving from pH 8.3 to 5.0.[9] According to our results, protonation of the isolated resting cofactor leads to the aquo complex **1**, which spontaneously evolves to **2**. Remarkably, the computed UV−vis spectra for **1** and **2** differ considerably, with the former being in good agreement with experimental observations. This suggests that in the protein the aquo complex **1** is stabilized relative to **2**, an observation that is compatible with the nature of the cofactor environment in the protein, where several positively charged amino acids can withdraw electron density from the cofactor and stabilize the $V-OH_2$ bond observed in **1**.

Spectroscopic investigations revealed also that the addition of H_2O_2 results in a significant decrease of the band at 315 nm and appearance of a very small band at 384 nm.[9] Analysis of the corresponding computational data shows that the only peroxo form of the cofactor compatible with this experimental data is **7**, in very good agreement also with NMR observations[8] and with our computational evidences indicating that conversion from the initial intermediate formed upon hydrogen peroxide binding (**4**) to the side-on peroxo form (**7**) is thermodynamically favored and kinetically facile. Interestingly, the comparison of computed spectra for **7** and **7H**$^+$ (Figure 10) reveals that protonation of the peroxo moiety should lead to the appearance of a UV−vis band around 300 nm, a fingerprint that could be important in the interpretation of data from future experimental kinetic and spectroscopic investigations.

A two-step oxidation mechanism was previously proposed for halide oxidation/HOBr release.[9] However, while halide oxidation has been extensively investigated by quantum chemical methods,[32,38] little is known about species formed after Br^- oxidation.

The product of Br^- oxidation in which BrO^- is coordinated in an axial position corresponds to a stable species (**8**). Closure of the catalytic cycle and formation of the resting form of the cofactor implies reaction with a water molecule and release of HOBr (Scheme 4). Notably, also in this step an associative mechanism in which H_2O binding is concomitant to HBrO release is predicted to be highly unlikely due to the extremely high reaction barriers (Table 1). On the other hand, release of HBrO and formation of the four coordinate species **2** is facile when a water molecule mediates proton transfer from an equatorial hydroxo group to BrO^-.

(52) Mitchell, A. D.; Cross, L. C. *Table of interatomic distances and configuration in molecules and ions*; The Chemical Society: London, Burlington House, 1958.

Conclusions

The DFT investigation of key reaction steps involving the isolated vanadium cofactor found in VHPOs has allowed us to unravel structure−function relationships that are crucial to understand the catalytic activity of the enzyme better. These studies will also aid the design of novel functional biomimetic catalysts. In particular, (i) protonation of $[V(OH)_2(O)_2Im]^-$ is a key step in the activation of the cofactor, (ii) reaction between $[V(H_2O)(OH)(O)_2Im]$ and H_2O_2 takes place according to a dissociative mechanism and spontaneously leads to the side-on peroxo-species $[V(OH)(O)_3Im]$, (iii) an acid−base catalysts strongly accelerates the conversion from the initial H_2O_2 adduct to the side-on peroxo form, and finally, (iv) computed UV−vis spectra explained the effects of the vanadium ligands on the electronic properties of the cofactor and indirectly pointed out subtle effects of the protein environment.

Supporting Information Available: Computed electronic transitions. This material is available free of charge via the Internet at http://pubs.acs.org.

IC060555G